archives
of thermodynamics
Vol. **43**(2022), No. 3, 63–84
DOI: 10.24425/ather.2022.143172

Experimental analysis on unsteady characteristics of sheet/cloud cavitating Venturi flow under the effect of dissolved air

EMAD HASANI MALEKSHAH*
WŁODZIMIERZ WRÓBLEWSKI
KRZYSZTOF BOCHON
MIROSŁAW MAJKUT
KRZYSZTOF RUSIN

Silesian University of Technology, Department of Power Engineering and Turbomachinery, Konarskiego 18, 44-100 Gliwice, Poland

Abstract The highly dynamic and unsteady characteristics of the cavitating flow cause many negative effects such as erosion, noise and vibration. Also, in the real application, it is inevitable to neglect the dissolved air in the water, although it is usually neglected in the previous works to reduce the complexity. The novelty of the present work is analysing the impact of dissolved air on the average/unsteady characteristics of Venturi flow by conducting sets of experimental tests. For this purpose, two different amounts of dissolved air at five pressure levels (i.e. five different sets of cavitation numbers) were considered in the study of cavitating flow inside a Venturi nozzle. The fast Fourier transform analysis of pressure fluctuations proved that the shedding frequency reduces almost by 50% to 66%, depending on the case, with adding the amount of dissolved air. However, the reduction of 14% to 25% is achieved by the vibration transducers. On the other hand, the cavity enlarges as well as bubbly flow is observed in the test chamber at a higher level of dissolved air. Furthermore, it is observed that the re-entrant jet, as the main reason for the cavity detachment, is more effective for the detachment process in cases with a lower level of dissolved air, where the re-entrant jet front penetrates more toward the leading edge.

Keywords: Cavitating flow; Venturi nozzle; Dissolved air; Unsteady characteristic; Experimental observation

*Corresponding Author. Email: emad.hasani@polsl.pl

Nomenclature

A	–	area
C_p	–	pressure coefficient
H	–	height
L	–	length
p	–	pressure
q	–	flow rate
t	–	evolution time
t_0	–	onset time of cavitation
Re	–	Reynolds number
u	–	velocity
W	–	width
x	–	coordinate along the cavitation chamber axis

Greek symbols

μ	–	dynamic viscosity
σ	–	cavitation number
τ	–	one ninth of a period

Subscripts

in	–	inlet
l	–	liquid
th	–	throat
sat	–	saturation

1 Introduction

Cavitation is known as a sudden phase change phenomenon, which usually can be observed in high-speed flow and is due to low-pressure regions falling below the local saturation pressure of the operating fluid. This phenomenon exists in many applications such as hydro-power turbines, high-speed propellers, pumps and rockets [1–4]. The existence of highly dynamic cavitating flow, in particular with intensive cavity breakup, may lead to severe destructive effects such as erosion on the surface of the object, vibration, noise and high-frequency pressure fluctuations [5–10].

The Venturi-type sections and foils have been usually employed to study the unsteady cavitating flow and measure the corresponding parameters. These investigations help the researchers to improve their understanding of this phenomenon. Chen *et al.* [8] investigated the cavitation evolution based on experimental and numerical tests to evaluate the influence of exciting pressure fluctuations within a convergent-divergent Venturi nozzle.

They used a modified RNG k-ε turbulence model to predict the dynamics of cavitating flow. It is confirmed by both numerical and experimental results that the quasi-periodic sheet-cloud cavitating flow has three main stages, which are: 1) attached cavity growth, 2) attached cavity shedding, 3) detached cavity growth and collapse. Also, it is reported that the main source of the pressure fluctuation is the acceleration originating from changes in cavity volume. In experimental work, Stutz and Reboud [11] analysed the cavitating flow structure as two-phase flow. They considered both types of quasi-steady sheet cavitation and unsteady cloud cavitating flow within a convergent-divergent nozzle. They measured the mean volume fraction of the cavity and the velocity distribution inside the cavity closure. In another work, Stutz and Reboud [12] demonstrated that the break-off of sheet cavity is due to the re-entrant jet which flows periodically upstream. Shi *et al.* [13] studied the cavitating flow inside a Venturi tube based on experimental and numerical approaches. They have considered two geometries with convergent angles of 19° and 45° to evaluate the influence of configuration on the local and global characteristics of Venturi flow. It is proved that the changing of convergent angle has a considerable impact on the generation of cavitation at the throat and the related local characteristics. The influence of several geometrical parameters on cavitation initiation detected by a hydrophone and microbubble formation monitored by a high-speed camera was explored mathematically and experimentally by Li *et al.* [14]. Regardless of the design of the Venturi tube, the flow resistance generated by cavitation increases linearly with the decreasing downstream cavitation number while the upstream cavitation number remains constant in the cavitation regime. Low cavitation inception and strong microbubble production come from a small outlet angle. Furthermore, the increased flow resistance and dissolved gas concentration were observed to increase the degree of microbubble generation. Niedźwiedzka *et al.* [15] carried out an analytical investigation on cavitating flow inside the Venturi tube. The purpose of this paper is to verify the similarity of the characteristics obtained and those described in the literature, as well as to verify the range of the obtained characteristics in relation to parallel diagrams. Both objectives were met, indicating that the quality of the previous experimental data is at least adequate for achieving the project's major goal: the development of numerical models of cavitating flow in a Venturi tube. Charrière and Goncalves [16] performed a numerical study on periodic cavitation shedding inside a Venturi tube. One-fluid compressible simulations of a self-sustained oscillating cavitation region forming along a Venturi geometry are shown in this study.

A void ratio transport equation model drives mass transfer between the phases. Travelling pressure waves' importance in the physical mechanism is demonstrated. The significance of considering a non-equilibrium condition for the vapour phase is also highlighted. Fang *et al.* [17] studied the cavity shedding mechanism in a Venturi tube based on the numerical analysis. A numerical investigation of a Venturi reactor is undertaken in this paper, based on experimental research, using a self-developed compressible cavitation phase-change solution to discover the shedding mechanism. The key characteristics and physical indicators of the re-entrant jet and bubbly shock mechanisms are explored using the quasi-periodic evolution of the cavity combined with the contour of stream velocity and pressure. The evolution of cavitation in a Venturi reactor with a long throat was discovered to be split into four stages: conception, development, two shedding stages and collapse. The separation between the cavity and the wall is the most prominent feature of the shedding mechanism caused by the re-entrant jet. Reisman *et al.* [18] studied the short period and significantly large amplitude during cloud cavitation collapse. They have detected several types of propagating structures, so-called bubbly shock waves. In addition, Leroux *et al.* [19] studied the pressure fluctuation originated from the unsteady cavitating flow. It is interestingly declared that the shock wave created by the collapse of the cloud cavity has probably contributed to the occurrence of the re-entrant jet. Wu *et al.* [20] conducted a couple of experiments to analyse the sheet cavity structure followed by bubbly flow within a convergent-divergent test section. They used fast pressure transducers to collect the pressure distribution and a high-speed camera to record the flow structures. It is indicated that the frequency of recurring sheet cavity has a reverse relationship with the velocity of inlet flow. Also, it is observed that the flow structure changes from vortex shedding included with entrapped thin cavities to sheet cavity producing cloud cavity by re-entrant jet. Barre *et al.* [21] carried out a combined numerical and experimental work in order to study the attached sheet cavity structure in Venturi geometries. They employed a new double optical probe and a novel data processing approach for the evaluation of the velocity distribution and void ratio of the cavity. When the experimental and numerical results are compared, it is interestingly indicated that the applied barotropic model predicts the local characteristics of the sheet cavity well. On the contrary, some discrepancies can be detected between numerical predictions and experimental measurements. Dular *et al.* [22] conducted some experiments to visualize the cavitating flow and the related characteristics that deal with its unsteady behaviour

influenced by the different scale ratios. This work was motivated by the vague data provided by experimental measurement inside a Venturi-type section which was scaled down 10 times [23]. A significant influence on the cavitation process is found on a small scale. Especially the height of the test section plays a major role in the dynamics of the re-entrant jet that drives the periodical shedding observed at a large scale.

The researchers have introduced many types of approaches to control the unsteady dynamic behaviour of the cavitating flow, like geometrical parameters, the flexibility of foil, and scale factor [24–27]. However, it is worth mentioning that the impact of dissolved air in the water and ventilation is not negligible. In some cases, they have a considerable effect on the structure of the cavity and unsteady characteristics. Kawakami *et al.* [28] calculated the pressure spectrum at the suction side for the NACA 0015 hydrofoil by considering two amounts of dissolved air including 6 ppm and 13 ppm. Based on the results, the considerable effect of dissolved air on the pressure spectrum trends is proved. Numerous peaks are observed for the case with high gas content regardless of cavitation number located between $\sigma/2\alpha = 2$ to 4, where σ and α show the cavitation number and angle of attack, respectively. Reversely, a steady behaviour is seen for $\sigma/2\alpha$ less than 4 when the gas content is low. Pham *et al.* [29] used pressure transducers and a high-speed camera to study the unsteady behaviour of the sheet/cloud cavity and the mechanism which can be employed to control its instability using obstacles and air injection. The results showed that applying an obstacle has a remarkable effect on reducing the amplitude of the pressure flections. Also, the structure of the cavity closure is changed by employing air injection as well as; the positive effect of air injection on suppressing the cloud cavitation is approved. Wang *et al.* [30] evaluated the characteristics of the unsteady sheet/cloud cavity in a convergent-divergent channel under the effect of air injection. They conducted a series of experiments in the 10° divergent section equipped with a ventilation slot located near the throat. They observed that the air injection from the throat into the sheet cavity causes suppression in the cavitating flow and pressure fluctuations. Also, the fast Fourier transform (FFT) analysis showed that the period of cavitation cycle and shedding frequency enhances and reduces, respectively, due to the air injection.

This experimental work aims to investigate the cavitating flow in a Venturi nozzle. The cavitation process is visualized using a high-speed video camera, and the unsteady characteristics of the cavitation phenomenon are measured employing the pressure and vibration transducers. The main pur-

pose of the present work is to investigate what is usually neglected in the research on cavitating flow that is the dissolved air influence on the local and global characteristics of the cavitation process.

2 Experimental installation

2.1 Test rig

The experimental tests were carried out using a hydraulic test setup equipped with a cavitation chamber fabricated at the laboratory of the Department of Power Engineering and Turbomachinery at the Silesian University of Technology. Figure 1 presents the main components used in the close-loop installation. The water flow is streamed by a pump with 30 kW power output in the pipe installation with 200 mm diameter. A manual valve and electromagnetic flowmeter are installed in the circuit after the pump to control the flow rate. It is to note that the cavitation test chamber is located about 5000 mm above the pump level. Then, the water passes through two 90° elbows. The honeycomb is installed before the inlet nozzle where the shape of the pipe alters from circular to rectangular. In addition, the dif-

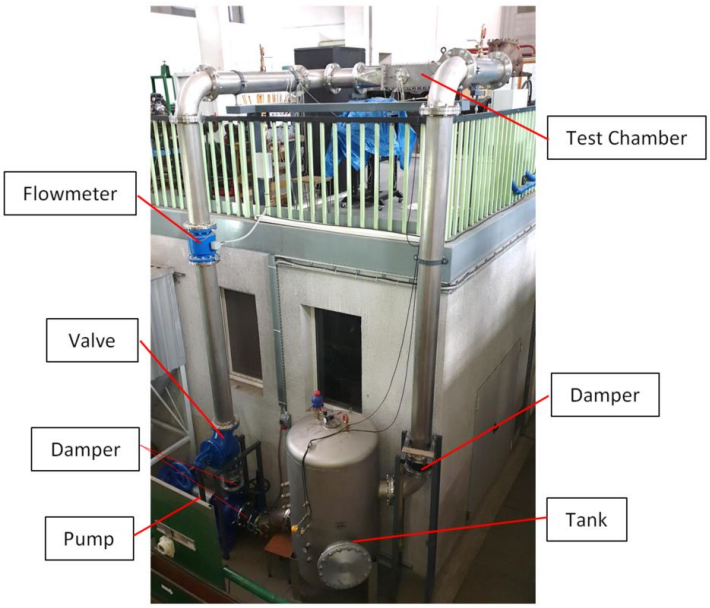

Figure 1: Closed-loop installation with the main components.

fuser is employed after the test chamber to change the pipe shape back to circular. Afterwards, the water flow passes two elbows and is headed to the tank fixed at the ground level. The capacity of the tank is about 1.5 m^3, which is designed to be able to control the pressure value. For this purpose, an internal elastic airbag is mounted at the top section inside of the tank. The airbag is connected with the compressed air system making it possible to be enlarged and with a release valve creating the control system to regulate the pressure level of the circuit. Based on the design of the present closed-loop circuit, the test can be run with a constant flow rate and different pressure values at the inlet to the test chamber. Three elastic couplings (damper) are used to damp the induced forces and vibration during the test campaign which are located before the tank, after the pump and one between the tank and pump.

The cavitation test chamber had a rectangular cross-section, as shown in Fig. 2. The transparent window, which was made of polycarbonate, was placed at the one sidewall of the test chamber to enable optical access and observations. The length (L), height (H) and width (W) of the chamber are equal to 700 mm, 189 mm and 70 mm, respectively. The length of Venturi throat (L_{th}) is equal to 113.5 mm, hence the ratio of throat length to height of the chamber is defined as $L_{th}/H \simeq 0.6$. The ratio of chamber height to width was fixed as $H/W = 2.7$.

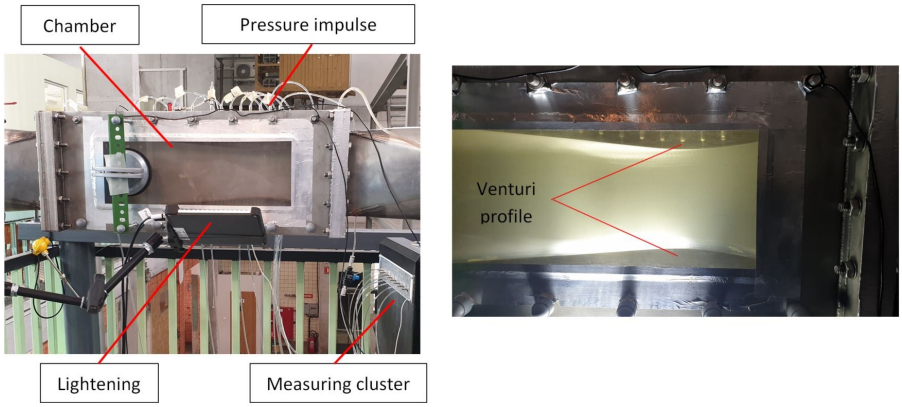

Figure 2: A view of cavitation test chamber including related components (left) and Venturi nozzle (right).

The schematic configuration of the Venturi nozzle included with internal channels and the location of pressure taps are represented in Fig. 3. The Venturi profile is equipped with 10 internal channels connecting the pres-

sure taps ($P1-P10$) at the surface of the Venturi nozzle to the pressure transducers. The diameter of pressure taps is equal to 1 mm. Moreover, two more pressure taps are installed at the inlet (P_{in}) and outlet (P_{out}). In addition, the vibration due to cavitating flow is measured using two vibration sensors installed at the back-side wall. As shown in Fig. 3 (right), the Venturi profiles at the bottom and top of the channel are the same. To show more details during the visualization process, only half of the Venturi nozzle is captured considering the fact that the cavitating flow is symmetric.

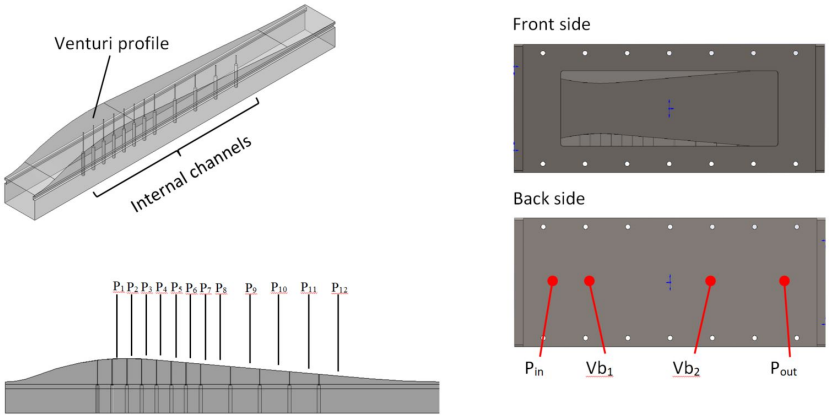

Figure 3: 3D view of Venturi profile (left) and the location of pressure taps (P) and piezoelectric transducers – accelerometers (Vb) (right).

2.2 Measurement system

The measuring system including a high-speed camera, image control, rig control, lightening and test chamber is shown in Fig. 4. The instantaneous pressure values at the surface of the top Venturi profile are measured with the low-frequency sampling rate by pressure transducers Aplisens PC-28. The accuracy of 0.16% is approved for the full scale amounting to 160 kPa. The pressure sensor type XP5 with amplifier ARD154 is used as a fast pressure sensor at pressure tap *P8*. The full scale of this type of sensor is given by 500 kPa with an accuracy of 0.25%. The pressure impulse tubes are used to send the pressure signal to the measuring cluster. Furthermore, the same low-frequency pressure sensors are used to measure the pressure level at the outlet. The temperature of the water is measured by the resistance thermometer Aplisens CT-GN1 Pt100, having a full scale of $0-100^{\circ}$C

and accuracy of $\pm(0.15\,\mathrm{K} + 0.002|\mathrm{T}|)$. The flow rate is measured by electromagnetic flowmeter UniEMP-05 DN200 with a measuring range up to 1080 m^3/h and accuracy of $\pm 0.25\%$ of the measured value.

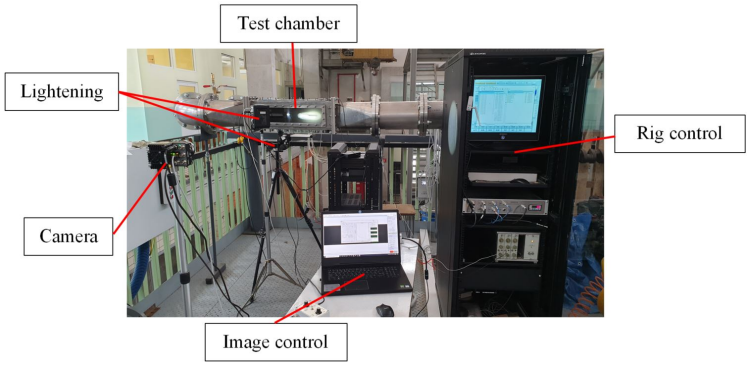

Figure 4: The measuring system including a high-speed camera, image control, rig control, lightening and test chamber.

The vibroacoustic signals were recorded from outside the chamber by two piezoelectric transducers. The two stiff piezoelectric accelerometers KD35 (RTF) are located externally on the sidewall of the test chamber. The Vb_1 is located about one profile chord before the leading edge and the second Vb_2 about one and a half chord behind the trailing edge, Fig. 3 (right). The accelerometers are connected with the 0028 (RFT) type charge amplifier connected with the fast response converter AC 16 bit, 250 kS/s. The system was calibrated before experiments using the electrodynamic vibration calibrator EET101 (RFT) type. The value of achieved limiting error was less than 5%.

The measurement system used in the research is based on a National Instruments module NI USB 6216. The NI/PXI-6255 module co-operates with measuring clusters which include sets of sensors and measuring transducers. The executive elements and the data acquisition process are managed by a system programmed in the LabView environment.

An important part of the data acquisition system is image recording and processing. The structures of cavitation were recorded by a high-speed video camera Phantom Miro C110. The recording speed was set to 3200 frames per second with a spatial resolution of 960×280 pixels. The settings of the camera resolution and speed were selected as a compromise between image quality and picture size.

2.3 Flow conditions

The volume flow rate of the circuit was kept constant in all rounds of experiments. So, the velocity of the stream is constant at the inlet, throat and outlet during the time, when the inlet velocity is calculated as $u_{\text{in}} = q/\rho_l A_{\text{in}} = 10.4$ m/s, where q, A_{in} represent the volume flow rate and area of inlet section, respectively. The Reynolds number is calculated as $\text{Re} = \dfrac{\rho_l u_{\text{in}} L_{th}}{\mu_l} \simeq 1.15 \times 10^6$, where ρ_l, u_{in}, L_{th}, and μ_l represent the density of water, velocity of flow at the inlet, length of Venturi throat, and dynamic viscosity of water, respectively.

The temperature of the water was between 27°C to 31°C at two successive rounds of the test campaign dealing with 4 different cavitation numbers (i.e. two contents of dissolved air and two pressure levels). The detected temperature differences were due to the friction between the stream and the pipe as well as differences in the ambient conditions, but not exceeded 2°C at each test campaign.

Each case with different inlet pressure, saturation pressure, density and inlet velocity, is defined with a single cavitation number calculated as follows:

$$\sigma = \frac{p_{\text{in}} - p_{\text{sat}}}{0.5\rho_l u_{\text{in}}^2}\,, \tag{1}$$

where p_{in} and p_{sat} denote the static pressure at the inlet and water saturation pressure, respectively. Also, the value of inlet pressure is based on the average pressure calculated from instantaneous pressure fluctuations during the round of the related experiment. Furthermore, the saturation pressure is calculated based on the average temperature calculated over the related experiment. Also, ρ_l shows the density of water calculated at the corresponding temperature and pressure at each case with the nominal cavitation number. Finally, u_{in} represents the velocity at the inlet, which is also based on the average value.

In the present work, five levels of rig pressure (150, 155, 160, 165, and 170 kPa), which are categorized with different names as PT150, PT155, PT160, PT165, and PT170 and represented by cavitation number, and two air contents (i.e high and low) are studied. It should be noted that two first letters is abbreviation of pressure transducer (PT), and the number denotes the pressure level. The corresponding cavitation number for each case is presented in Table 1.

Table 1: Cavitation numbers for the experimental cases.

	Case name				
	PT150	PT155	PT160	PT165	PT170
Air content	Cavitation number				
Low: 6.13 mg/l	2.01	2.04	2.10	2.20	2.33
High: 14.83 mg/l	2.04	2.07	2.08	2.18	2.35

The experimental tests are conducted based on two levels of dissolved oxygen of 2.4 mg_O_2/l and 5.8 mg_O_2/l. The multifunction meter CF-401 is employed to measure the oxygen levels before and after each experimental campaign. The average value of the oxygen is reported in this work. Based on Henry's law, it corresponds to the air content of 6.13 mg_air/l and 14.83 mg_air/l, respectively.

3 Results and discussion

The main aim of the present experimental work is to investigate the effect of dissolved air on the cavitating flow inside a Venturi nozzle. Two amounts of air content, so-called high and low levels, with 6.13 mg_air/l and 14.83 mg_air/l, respectively; and five levels of rig pressure were taken into consideration. Thus, five sets of cavitation numbers, as presented in Table 1, are taken into consideration. The evolution of the cavitation process was visualized using a high-speed camera and image processing. In addition, the unsteady characteristics of cavitating flow such as pressure fluctuation and vibration were recorded using pressure and vibration transducers. The FFT analysis was employed to detect the main frequency of shedding.

3.1 Pressure coefficient distribution

The pressure coefficient distributions for different cavitation numbers are presented in Fig. 5. The presented pressure coefficient distribution is based on the measured pressure values at the surface of the Venturi profile and calculated as follows:

$$C_p = \frac{p - p_{\text{in}}}{0.5\rho_l u_{\text{in}}^2}\,. \tag{2}$$

It is observed that there is a strong pick near the throat in all cases. In the cases with a higher air content, the difference of the pressure coefficient correspondence to different cavitation numbers is more significant. In the

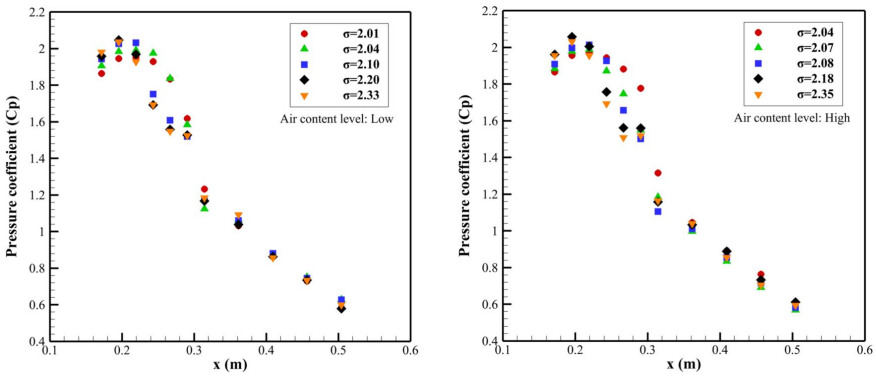

(a) (b)

Figure 5: Pressure distribution coefficient at the surface of Venturi nozzle along the cavitation test chamber axis as a function of cavitation number at two air contents.

case with lower air content, the flat distribution of pressure coefficient is observed in a very small region close to the throat. By increasing the amount of dissolved air, the flat distribution extended for all cases, especially the one with a lower cavitation number. It means that the cavity closure elongated through the channel. In addition, the sudden pressure drop is due to the transition from sheet cavity to cloud cavity since there is a considerable pressure difference between inside and outside of the cavity closure.

3.2 Fast Fourier transform analysis

In Fig. 6, the fast Fourier transform (FFT) analysis is employed to extract the frequency associated with the unsteady behaviour of the cavitating flow over different cavitation numbers. The FFT analysis is based on the pressure fluctuation measured by the fast pressure sensor located at P_8 and vibration fluctuations collected by the sensor Vb_2. Using the provided FFT analysis, it is possible to detect the influence of air content and cavitation number on the rate of cavity evolution. It is expected that the frequency of shedding would enhance with the cavitation number since smaller cavities oscillate faster than larger ones. This is what is concluded by the present FFT analysis for lower air content, but is not applied to the higher one. In addition, the FFT analysis of vibration approves the reverse relationship of the cavitation number and frequency. In low air content, the frequency provided by vibration FFT analysis reduces from 8 Hz to 6 Hz as the cavita-

tion number enhances. No difference is detected in the vibration frequency at the higher air content. On the other hand, the changes in the frequency of cavitation cloud shedding, dealing with different air contents, are more observable in the lower cavitation number. The shedding frequency reduces when the air content rises. Thus, one can conclude that increasing air content results in stabilization of the cavitation flow as the cavity evolution lasts longer.

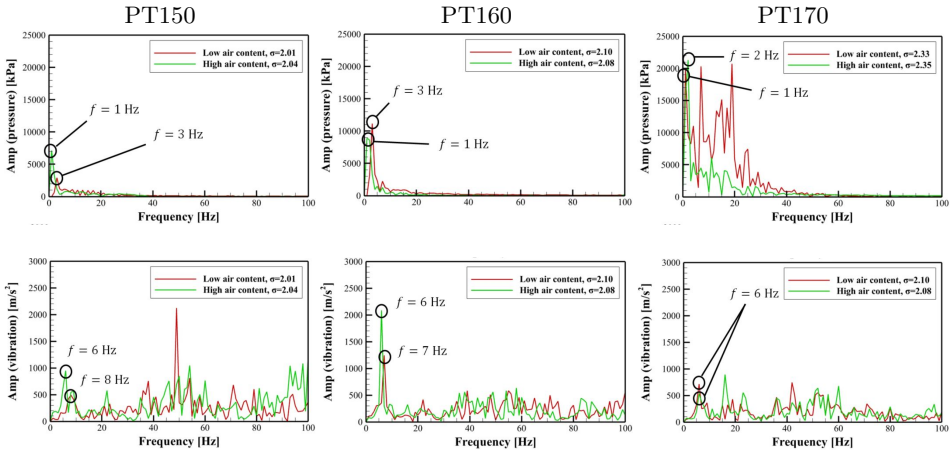

Figure 6: FFT analysis based on pressure fluctuation collected by fast pressure sensor $P8$ and vibration transducer Vb_2.

3.3 Pressure and vibration fluctuations

Figure 7 shows the instantaneous pressure fluctuation collected by the fast pressure sensor (P_8) and vibration sensor (Vb_2). Firstly, the collected data show the high dynamic behaviour and unsteady characteristic of the cavitating flow. Based on the fluctuation plots, it can be concluded that the unsteadiness and the cavitation number have a reverse relationship since the pressure difference between the minimum and maximum peaks is higher in the cases with lower cavitation number. Furthermore, the stronger unsteadiness of the cavitating flow at a lower cavitation number can be concluded by the vibration fluctuation, where the average difference between the minimum and maximum points is higher than in other cases. On the other hand, the higher level of dissolved air in water results in a stable cavitation process, which is proved by comparing the pressure and vibration ranges.

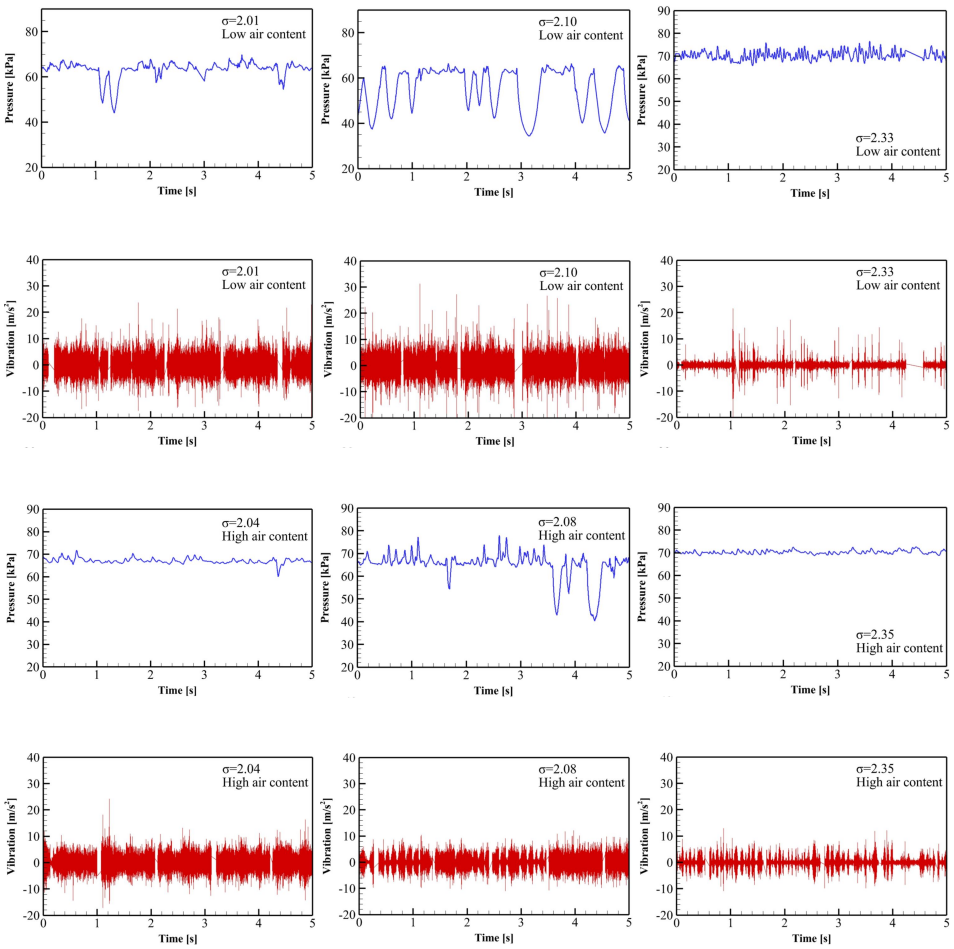

Figure 7: Pressure and vibration fluctuations for different air volume fractions and cavitation numbers.

3.4 Cavity evolution visualization

The evolutions of cavitating flow over one period are presented in Figs. 8–9, where t, t_0, and τ present the evolution time, onset time of cavitation and one ninth of a period, respectively. Based on the presented visualizations, significant influence on the cavitation flow is observed considering various air contents and pressure levels. Thus, the cavity evolution is required to be studied from both points of view, separately. Comparing the cases at lower and higher pressure levels, it may be understood that the area of

cavity closure is elongated and covers a larger area of the channel when the pressure level is lower.

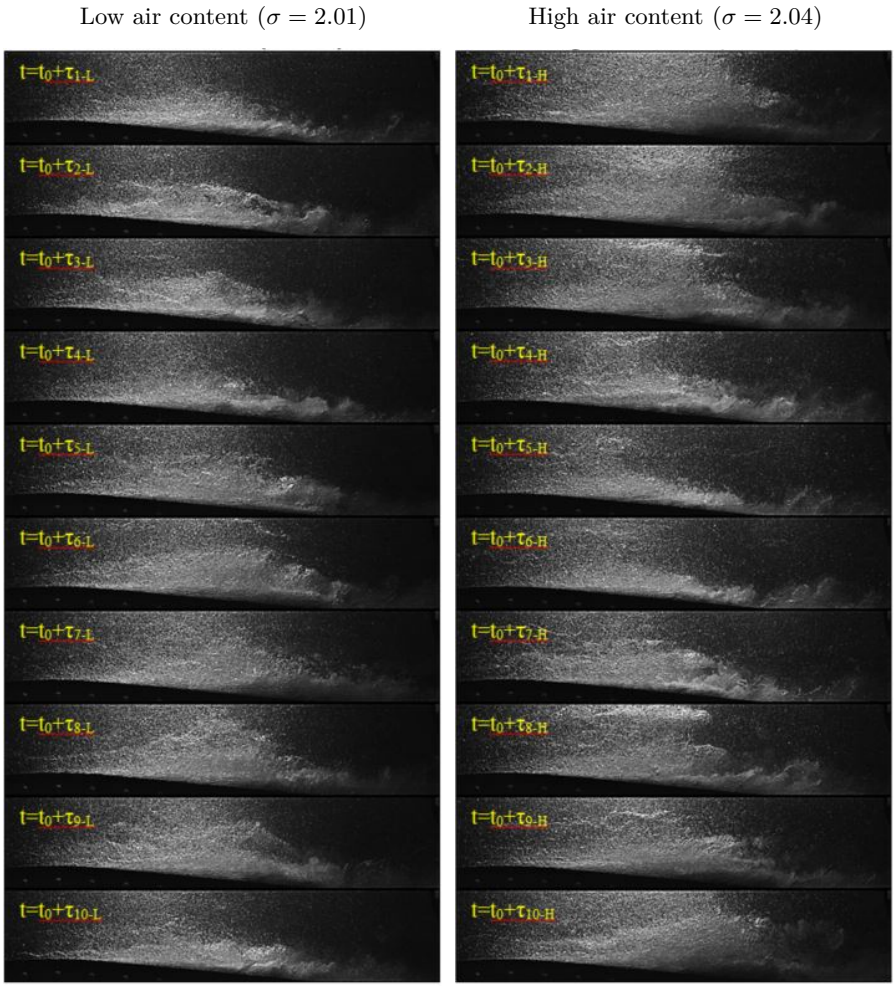

Figure 8: Experimental visualization of cavity evolution in one period for PT150.

At the low pressure level, it is observed that the steady cloud cavity exists during the period. On the contrary, when the pressure level increases, no cloud cavity can be found in some time intervals. Furthermore, it is hard to recognize the detachment and shedding process in the case with the high pressure level. Hence, the air content in the water has a remarkable influence on the size, frequency and configuration of the cloud cavity. Liquids

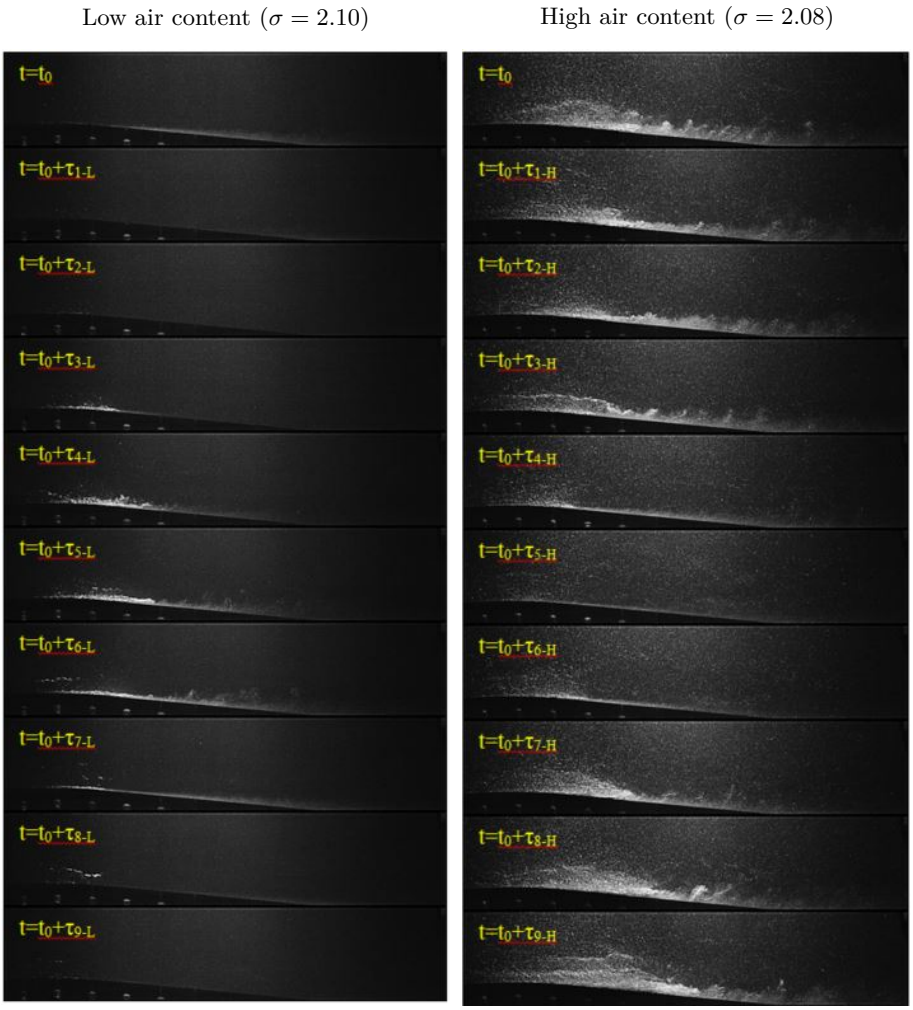

Figure 9: Experimental visualization of cavity evolution in one period for PT160.

and solids exhibit practically no change in solubility with changes in pressure. Gases as might be expected, increase in solubility with an increase in pressure. Henry's law states that the solubility of a gas in a liquid is directly proportional to the pressure of that gas above the surface of the solution. If the pressure is increased, the gas molecules are "forced" into the solution since this will best relieve the pressure that has been applied. The relationship between pressure and the solubility of a gas as described quantitatively by Henry's law can be defined as $C = kP$, where C denotes

the concentration of dissolved gas at equilibrium, P shows the partial pressure of the gas and k is Henry's law constant. Thus, it is expected that the dissolved air releases from the water partially in the regions with low pressure. It is known that the local pressure inside the cavity is lower than in other regions, which results in decreasing the solubility. The released dissolved air causes the creation of a larger sheet cavity. In addition, a larger sheet cavity can be easier detached by the re-entrant jet. Overall, it is likely to have a larger cloud cavity with a faster shedding process. This can be observed in the visualized cavity evolution, as the larger cavity exists during the period for all cavitation numbers.

3.5 Influence of dissolved air on re-entrant jet

Figure 10 shows the evolution of the re-entrant jet based on the dissolved air content for PT150. In the present figure, the cavity region, including the

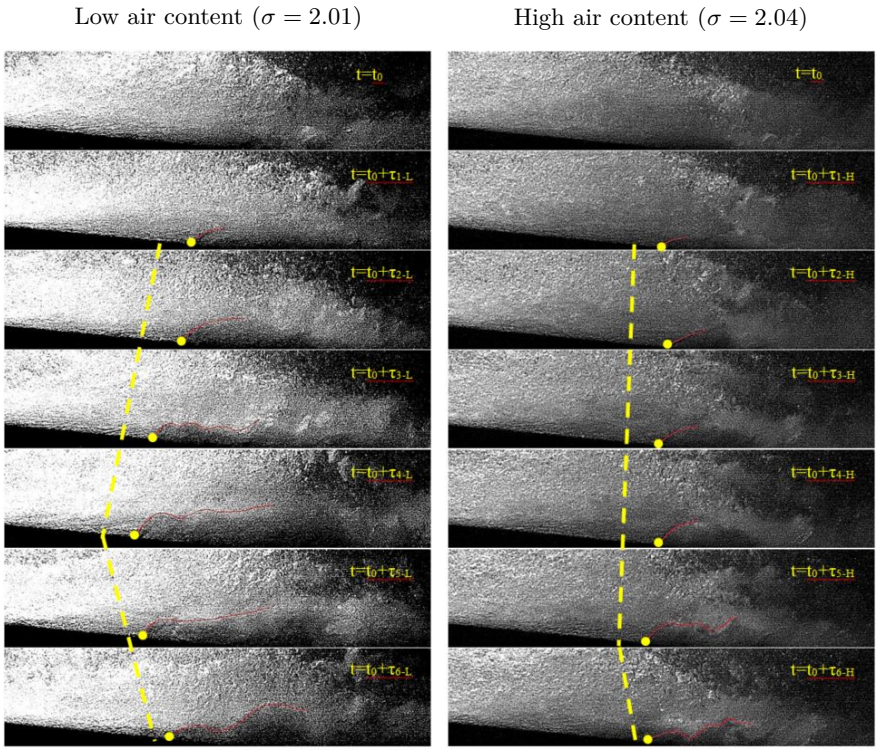

Figure 10: Influence of dissolved air volume fraction on the re-entrant jet for PT150.

sheet and cloud cavity, are shown with white and grey colours depending on the density of the bubble, and the pure water can be detected in black colour. The periodic shedding of cavitation cloud is one form of cavitation instability common to both external bodies and internal cavitating flows. The transient nature of the instability is known to be dependent upon a liquid sublayer referred to as a re-entrant jet. Despite the importance of the re-entrant jet, the mechanism by which it controls the periodic motion is not entirely understood. As a result, it is worth keeping this phenomenon under investigation dealing with different influential parameters. The re-entrant jet establishes when the vapour vortex inside the cavity becomes strong. Then, the re-entrant jet flows upstream along the nozzle wall toward the throat. In the present figure, one can characterize the re-entrant jet when the grey level of pixels slightly reduces to the black level. Hence, it is to note that the re-entrant jet mainly consists of pure liquid. On the other hand, not all of the re-entrant jets can change the type of cavity from sheet to cloud, but just the ones with strong momentum. It is required for the re-entrant jet to penetrate enough beneath the sheet cavity to be able to detach it. Overall, when the re-entrant jet arrives at the rear front of the sheet cavity and penetrates enough on it, it will cut off the sheet cavity and detach the whole or part of it. The detached portion of the sheet cavity moves downstream and collapses in the high-pressure region. As shown in Fig. 10, the re-entrant jet moves upstream and detaches parts of the sheet cavity, and then it deteriorates and moves back when its momentum gets low. With increasing the dissolved air content, the penetration level of the re-entrant jet reduces compared to the case with lower air content. This causes less cloud cavity and collapse and more sheet cavity, which improves the stability of the cavitating flow.

Figure 11 represents the result of image processing to show the effect of dissolved air content on the cavity length. This analysis is performed for three cases of PT140, PT150 and PT160 for both levels of air contents (i.e. low and high air contents). Calculation of the normalized cavity area was performed based on the colour-filtering technique. Figures like Fig. 11 were used to analyze the total share of black, white and grey pixels in the image. Thus, the normalized cavity (NCA) area was calculated as NCA = 1 − (black area %/100). When employing this parameter, it was possible to make a relative comparison between the cavity areas. It is declared that the length of the cavity has a direct relationship with the level of dissolved air. As the level of dissolved air increases, the cavity length enlarges in all cases.

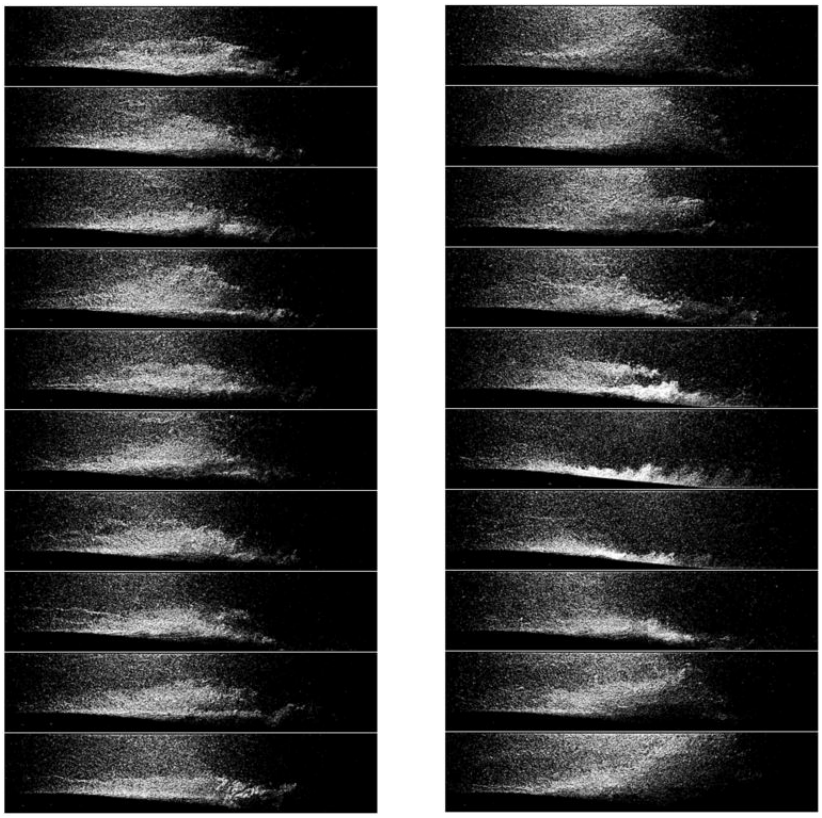

(a) (b)

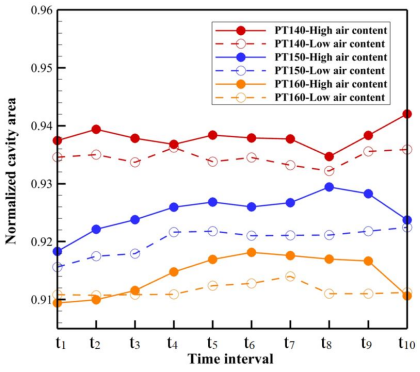

(c)

Figure 11: Sample of cavity area detection over a period based on colour-filtering process: (a) PT140 – low air content, (b) PT140 – high air content; (c) a quantitative result of normalized cavity area over a time period.

4 Conclusion

The present work aims to investigate the cavitating flow inside a Venturi nozzle. The influence of the dissolved air in the water and two pressure levels (i.e four different cavitation numbers) is taken into consideration. The experimental observations are carried out in the closed-loop cavitation tunnel located at the Department of Power Engineering and Turbomachinery of the Silesian University of Technology. Also, the high-speed camera and image processing are used to visualize the cavity structure and evolution. In addition, the pressure and vibration transducers are employed to collect the local instantaneous characteristics of the cavitation process. The following key results have been concluded:

1. The periodical behaviour of internal cavitating flow around the Venturi nozzle is proved using pressure and vibration fluctuations.

2. The shedding frequency is in the range of 2–3 Hz and 1–2 Hz in the cases with low and high air contents.

3. Based on the fast Fourier transform analysis of pressure fluctuation, the shedding frequency reduces between 50% to 60%, depending on the case, when the air content increases.

4. The reduction of 14% to 25% is observed for shedding frequency recorded in the FFT of vibration plots.

5. The cavity closure is elongated with the increasing content of dissolved air.

6. The re-entrant jet plays a more important role to generate the cloud cavity at low dissolved air content.

7. A larger sheet attached cavity is found in cases with a high dissolved air content.

Acknowledgement The presented work was supported by the Polish National Science Centre within the project UMO-2016/21/B/ST8/01164.

Received 24 February 2022

References

[1] Brennen C.E.: *Cavitation and Bubble Dynamics*. Cambridge Univ. Press, 2014.

[2] Malekshah E.H., Wróblewski W., Bochon K., Majkut M.: *Evaluation of modified turbulent viscosity on shedding dynamic of three-phase cloud cavitation around hydrofoil–numerical/experimental analysis*. Int. J. Numer. Method. H. (in press).

[3] Wróblewski W., Bochon K., Majkut M., Malekshah E.H., Rusin K., Strozik M.: *An experimental/numerical assessment over the influence of the dissolved air on the instantaneous characteristics/shedding frequency of cavitating flow. Ocean Eng.* **240**(2021), 109960.

[4] Niedźwiedzka A., Schnerr G.H., Sobieski W.: *Review of numerical models of cavitating flows with the use of the homogeneous approach*. Arch. Thermodyn. **37**(2016), 2, 71–88.

[5] Joseph D.D.: *Cavitation in a flowing liquid. Phys. Rev. E,* **51**(1995), 3, R1649-R1650. https://doi.org/10.1103/PhysRevE.51.R1649.

[6] Paik B.-G., Kim K.-S., Kim K.-Y., Ahn J.-W., Kim T.-G., Kim K.-R., Jang Y.-H., Lee S.-U.: *Test method of cavitation erosion for marine coatings with low hardness*. Ocean Eng. **38**(2011), 13, 1495–1502.

[7] Chen G., Wang G., Hu C., Huang B., Zhang M.: *Observations and measurements on unsteady cavitating flows using a simultaneous sampling approach*. Exp. Fluids **56**(2015), 2, 1–11.

[8] Chen G., Wang G., Hu C., Huang B., Gao Y., Zhang M.: *Combined experimental and computational investigation of cavitation evolution and excited pressure fluctuation in a convergent–divergent channel*. Int. J. Multiphas. Flow **72**(2015), 133–140.

[9] Simpson A., Ranade V.V.: *Modeling hydrodynamic cavitation in venturi: Influence of venturi configuration on inception and extent of cavitation*. AIChE J. **65**(2019), 1, 421–433.

[10] Wróblewski W., Bochon K., Majkut M., Rusin K., Malekshah E.H.: *Numerical study of cavitating flow over hydrofoil in the presence of air*. Int. J. Numer. Method. H. **32**(2021) 5, 1440–1462.

[11] Stutz B., Reboud J.: *Experiments on unsteady cavitation*. Exp. Fluids **22**(1997), 3, 191–198.

[12] Stutz B., Reboud J.L.: *Two-phase flow structure of sheet cavitation*. Phys. Fluids. **9**(1997), 12, 3678–3686.

[13] Shi H., Li M., Nikrityuk P., Liu Q.: *Experimental and numerical study of cavitation flows in venturi tubes: From CFD to an empirical model*. Chem. Eng. Sci. **207**(2019), 672–687.

[14] Li M., Bussonničre A., Bronson M., Xu Z., Liu Q.: *Study of Venturi tube geometry on the hydrodynamic cavitation for the generation of microbubbles*. Miner. Eng. **132**(2019), 268–274.

[15] Niedźwiedzka A., Sobieski W.: *Analytical analysis of cavitating flow in Venturi tube on the basis of experimental data*. Tech. Sci. **19**(2016), 3, 215–229.

[16] Charričre B., Goncalves E.: *Numerical investigation of periodic cavitation shedding in a Venturi*. Int. J. Heat Fluid Fl. **64**(2017), 41–54.

[17] Fang L., Li W., Li Q., Wang Z.: *Numerical investigation of the cavity shedding mechanism in a Venturi reactor*. Int. J. Heat Mass Tran. **156**(2020), 119835.

[18] Reisman G., Wang Y.-C., Brennen C.E.: *Observations of shock waves in cloud cavitation*. J. Fluid Mech. **355**(1998), 255–283.

[19] Leroux J.-B., Astolfi J. A., Billard J.Y.: *An experimental study of unsteady partial cavitation*. J. Fluids Eng. **126**(2004), 1, 94–101.

[20] Wu X., Maheux E., Chahine G.L.: *An experimental study of sheet to cloud cavitation*. Exp. Therm. Fluid Sci. **83**(2017), 129–140.

[21] Barre S., Rolland J., Boitel G., Goncalves E., Patella R.F.: *Experiments and modeling of cavitating flows in Venturi: attached sheet cavitation*. Eur. J. Mech. B-Fluid. **28**(2009), 3, 444–464.

[22] Dular M., Khlifa I., Fuzier S., Maiga M.A., Coutier-Delgosha O.: *Scale effect on unsteady cloud cavitation*. Exp. Fluids **53**(2012), 5, 1233–1250.

[23] Coutier-Delgosha O., *et al.*: *Local measurements in cavitating flow by ultra-fast X-ray imaging*. In: Proc. Fluids Engineering Division Summer Meet. **43734**(2009), 371–379.

[24] Xu S., Wang J., Cheng H., Ji B., Long X.: *Experimental study of the cavitation noise and vibration induced by the choked flow in a Venturi reactor*. Ultrason. Sonochem. **67**(2020), 105183.

[25] Long X., Zhang J., Wang J., Xu M., Lyu Q., Ji B.: *Experimental investigation of the global cavitation dynamic behavior in a venturi tube with special emphasis on the cavity length variation*. Int. J. Multiphas. Flow **89**(2017), 290–298.

[26] Tomov P., Khelladi S., Ravelet F., Sarraf C., Bakir F., Vertenoeuil P.: *Experimental study of aerated cavitation in a horizontal Venturi nozzle*. Exp. Therm. Fluid Sci. **70**(2016), 85–95.

[27] Kozák J., Rudolf P., Hudec M., Urban O., Štefan D., Huzlík R., Čala M.: *Investigation of the cavitation within venturi tube: influence of the generated vortex*, In: Advances in Hydroinformatics. Springer, 2018, 1049–1067.

[28] Kawakami D.T., Qin Q., Arndt R.: *Water quality and the periodicity of sheet/cloud cavitation*. In: Proc. Fluids Engineering Division Summer Meet. **41995**(2005), 513–517.

[29] Pham T., Larrarte F., Fruman D.H.: *Investigation of unsteady sheet cavitation and cloud cavitation mechanisms*. J. Fluids Eng. **121**(1999), 2, 289–296.

[30] Wang C., Huang B., Zhang M., Wang G., Wu Q., Kong D.: *Effects of air injection on the characteristics of unsteady sheet/cloud cavitation shedding in the convergent-divergent channel*. Int. J. Multiphas. Flow **106**(2018), 1–20.